Fracture and Fatigue Behaviour of Epoxy Nanocomposites Containing 1-D and 2-D Nanoscale Carbon Fillers

Raj B. Ladani[1], Mukesh Bhasin[1], Shuying Wu[2], Anil R.Ravindran[1], Kamran Ghorbani[1], Jin Zhang[3]

Anthony J. Kinloch[4*], Adrian P. Mouritz[1], and Chun H. Wang[1,2]

[1]Sir Lawrence Wackett Aerospace Research Centre, School of Engineering, RMIT University, GPO Box 2476, Melbourne, VIC 3001, Australia.

[2]School of Mechanical and Manufacturing Engineering, University of New South Wales, Sydney, NSW 2052, Australia.

[3]Institute for Frontier Materials, Deakin University, Geelong Waurn Ponds Campus, VIC 3220, Australia

[4]Department of Mechanical Engineering, Imperial College London, South Kensington Campus, London SW7 2AZ, UK.

Abstract

The present paper describes improvements in the fracture resistance of epoxy polymers due to the addition of either (a) one-dimensional (1-D) carbon nanofibres (CNFs), or (b) two-dimensional (2-D) graphene nanoplatelets (GNPs), or (c) hybrid combinations of these carbon nanofillers (i.e. using both CNFs and GNPs). The effects of the dimensional shape and concentration (i.e. 0.0, 0.5, 1.0, 1.5 and 2.0 wt%) of the nanoscale carbon fillers are considered. The addition of CNFs, GNPs or hybrid combinations of CNFs and GNPs increases greatly the quasi-static fracture energy, G_{Ic}, of the epoxy due to these nanofillers inducing multiple intrinsic (e.g. interfacial debonding and void growth) and extrinsic (e.g. pull-out and bridging) toughening mechanisms. A mechanistic model is presented to quantify the contributions from the different toughening mechanisms induced by the CNF and the GNP fillers which result in the improvements observed in the fracture energy. The resistance of the epoxy, modified with either the GNPs or the CNFs, to cyclic-fatigue loading is also increased by the presence of the carbon nanofillers.

Keywords: Epoxies, Fatigue behaviour, Fracture energy, Modelling, Nanocomposites

*Corresponding author

1. Introduction

Thermosetting polymers, such as epoxies, are used in a wide range of adhesive, fibre-reinforced composite and coating applications. Despite having many desirable properties, unmodified epoxies usually have a relatively low toughness and poor cyclic fatigue resistance, which can led to rapid and large-scale cracking.

Now, nanoscale carbon fillers can improve the performance of polymers [1, 2] and, especially relevant to the present study, is that they may increase the toughness of thermosetting epoxies. For example, graphene nanoplatelets (GNPs) [e.g. 3-5], carbon nanotubes (CNTs) [e.g. 6-7] and carbon nanofibres (CNFs) [e.g. 8-10] have all been shown to increase the fracture energy of epoxies. In addition, carbon nanofillers increase the matrix-dominated properties of fibre-reinforced polymer composites, such as the inter- and intra-ply mechanical properties [e.g. 11-14]. There have also been studies [15-21] that have investigated the effects of a combination of carbon nanofillers on the fracture properties. The idea of using a combination of carbon nanofillers, to give a hybrid-modified polymer, is based upon research that has shown that synergistic improvements to the toughness of epoxy composites can be achieved with hybrid combinations of short carbon-fibres and CNFs [22] and short carbon-fibres and CNTs [23]. However, to the best of the authors' knowledge, no studies on hybrid combinations of CNFs and GNPs to improve the toughness of polymers have yet been reported.

Further, studies on the cyclic-fatigue properties of epoxies containing one-dimensional (1-D) carbon nanofillers, such as CNTs and CNFs, have reported good improvements to the fatigue resistance due to a multitude of toughening mechanisms induced by such nanofillers [24-28]. These studies demonstrated that the fatigue resistance increased with the concentration, up to a limiting content, of the CNTs [26,27] or CNFs [28]. Similarly, others have reported an improvement to the fatigue properties of epoxies containing two-dimensional (2-D) carbon nanoplatelet fillers, such as graphene or graphene oxide [4,11]. However, these fatigue studies were limited to a single concentration of graphene nanofiller in the epoxy. Thus, the detailed effects of the concentration of graphene nanoplatelets on the fatigue properties of an epoxy remains unknown. Moreover, since the aforementioned studies on 1-D and 2-D carbon nanofillers were performed

using different epoxies, it is therefore difficult to draw a direct quantitative comparison between the fatigue performance and the toughening mechanisms operating in these different nanocomposite materials.

In the present paper, we aim to identify the effects of the shape and the concentration of carbon nanofillers on the mode I fracture energy and cyclic-fatigue properties of epoxy nanocomposites. This study involves a comparative assessment of 1-D CNFs, 2-D GNPs and hybrid combinations of the CNFs and the GNPs to modify an epoxy which possesses a relatively low toughness. Firstly, improvements to the fracture energy resulting from the addition of various concentrations of the carbon nanofillers in the epoxy are measured and compared. Secondly, the toughening mechanisms induced by the carbon nanofillers that are responsible for the measured improvements to the fracture energy are identified. Thirdly, a mechanistic fracture model is presented to quantify the contributions of the different toughening mechanisms promoted by the CNFs and GNPs on the overall fracture energy of the epoxy nanocomposites. Finally, improvements to the quasi-static fracture energy and the cyclic-fatigue properties resulting from the addition of various concentrations of the carbon nanofillers in the epoxy are measured and compared.

2. Materials and experimental details

The carbon nanofillers used in this study were commercially-available carbon nanofibers (Pyrograf® - III, grade PR-24-XT-HHT supplied by Applied Sciences Inc.) and graphene nanoplatelets (xGnP, M grade supplied by XG Science). The CNFs had a diameter of about 70-200 nm and a length of 50-200 μm, and therefore had a length-to-width aspect ratio in the range of 250-2900, and are approximately of a one-dimensional shape. The GNPs had an average thickness of approximately 10 nm, and the platelet length and width were 25 μm. This translates to an in-plane aspect ratio of about 1, and due to their very small thickness they are essentially two-dimensional materials. The epoxy resin used was a liquid blend of bisphenol A and bisphenol F (‘105’ from West System) and the curing agent (‘206’ from West System) was a blend of aliphatic amines and aliphatic amine adducts based on diethylenetriamine and triethylenetetramine. The ratio of resin-to-hardener used for the epoxy system was 5-to-1 by weight. Carbon fibre reinforced plastic (CFRP) laminate substrates (150 x 250 x 2.65 mm) were made using 12 plies of unidirectional T700 carbon-fibre/epoxy prepreg (VTM 264 supplied by the Applied Composites Group).

The epoxy nanocomposites were produced containing 0.5, 1.0, 1.5 and 2.0 wt% of CNFs, GNPs and hybrid carbon nanofillers (where a 1:1 weight fraction of CNFs and GNPs was used). Firstly, the desired weight fractions of the CNFs and GNPs were mixed into the liquid epoxy resin, with no hardener added at this stage of the process. For the epoxy nanocomposites containing CNFs, dispersion-aiding surfactants (Disperbyk-191 and -192 supplied by BYK®) were added in a concentration that was equal to the weight of CNFs employed (i.e. CNFs:D-191:D-192 at weight ratio of 1:1:1). The dispersion of the carbon nanofillers in the epoxy resin was achieved using a three-roll mill (Dermamill 100) calendering process. Details of the three-roll mill dispersion technique are given in our earlier studies [5,9]. Following dispersion of the carbon nanofillers, the amine-based curing agent was added to the resin at the weight ratio of 1:5, and hand-mixed for approximately 5 minutes. This mixture was then poured between the carbon-fibre reinforced-plastic (CFRP) substrates to form a 2 mm thick adhesive layer bonding the two CFRP laminate substrates. The epoxy-resin nanocomposite layer was cured at room temperature (i.e. 25^{o}C) for 48 hours in accordance with the resin supplier's recommendations.

The unmodified epoxy and different types of epoxy nanocomposite joints were cut into double cantilever beam (DCB) coupons for mode I quasi-static fracture energy and cyclic-fatigue testing, as shown in **Fig. 1**. The details of the general procedure for testing and analysis of the DCB composite joints under quasi-static [9] and cyclic loading [28] were reported in our previous work. Essentially, the mode I fracture energy, G_{Ic}, was measured by testing the DCB specimens in accordance with the ISO standard [29]. The cyclic-fatigue testing was performed in accordance with the load-shedding scheme as prescribed in ASTM E647 [30]. The fatigue testing was performed under crack-opening displacement control at a constant amplitude, a sinusoidal cyclic ratio, *R*-ratio, of 0.5 and a frequency of 5 Hz. The DCB joints always failed by cohesive crack growth in the adhesive layer of the epoxy nanocomposite. A minimum of five replicate DCB specimens were used for the fracture energy tests and duplicate specimens were used to obtain the fatigue crack growth curves.

3. Results and discussion: Fracture energy of the epoxy nanocomposites

3.1 Values of the quasi-static fracture energy, G_{Ic},

Fig. 2 shows the effects of the type and weight fraction of the carbon nanofillers on the fracture energy, G_{Ic}, of the epoxy. The fracture energy increases almost linearly up to a nanofiller concentration of 1.5 wt%, although no further significant improvement occurs at the highest concentration of 2.0 wt% due to agglomeration of the nanofillers. For a given concentration of nanofillers, the increase in the fracture energy of the epoxy nanocomposites containing CNFs is generally higher than that measured for those nanocomposites containing the GNPs and the hybrid nanofillers. This was due to the difference in the extent of the toughening mechanisms induced by the CNFs and GNPs, which are discussed in detail in the following section.

3.2 Fracture toughening mechanisms

Fractographic analyses of the DCB specimens enabled the identification and quantification of the toughening mechanisms responsible for the improvements in the fracture energy of the epoxy nanocomposites. (It should be noted that, following the usual definition [31], 'intrinsic' toughening mechanisms are defined as those which operate ahead of the main crack front. Whilst 'extrinsic' toughening processes, which can shield the crack tip from the applied stress, are those which operate behind the crack tip.)

Fig. 3 shows a comparison of the side-view of the crack tip region for the unmodified epoxy and some epoxy nanocomposites and **Fig. 4** shows SEM images of the fracture surfaces. The crack tip in the unmodified epoxy is well-defined with no evidence of discrete damage processes ahead of the crack tip or extrinsic processes in the crack wake, and this is usually indicative of a low toughness material. In contrast, the process zone ahead of the crack tip in all the epoxy nanocomposites contains micro-scale damage (**Figs. 3b-c**). Micro-cracking occurred at many of the GNPs in the process zone, as shown in **Fig. 3d-e**. The high triaxial stress state that exists in the process zone led to the separation of the graphene layers within the multi-layered GNPs (see **Fig. 4f**), resulting in micro-cracking ahead of the crack tip. This type of micro-cracking mechanism was unique to the GNP containing epoxy nanocomposites. It did not occur with

respect to the CNF nanofillers since internal separation of the graphite sheets within the CNFs, which have a cone-helix structure [32, 33], did not occur within the process zone ahead of the crack tip. However, micro-cracking did also initiate via interfacial debonding of both the CNFs and the GNPs from the epoxy matrix. The interfacial bond strength between the carbon nanofillers and the epoxy is weaker than the covalent bond strengths within the epoxy. Consequently, under the triaxial stress field at the crack tip, the interfacial regions failed before the epoxy matrix, leading to micro-cracking within the process zone for the nanocomposites. These micro-cracks induced by the nanofillers will dissipate, within the process zone, some of the stored energy. Furthermore, the discrete micro-cracks within the process zone were observed to coalesce close to the main crack front, leading to crack branching occurring in the CNF and GNP epoxy nanocomposites (**Fig. 3e**). These relatively minor toughening mechanisms [34] may slightly increase the fracture energy of the epoxy nanocomposites.

Debonding of the CNFs or GNPs from the epoxy led to the formation of relatively large voids in the epoxy within the process zone (see **Fig. 4a-f**). The epoxy void growth mechanism occurs when the triaxial stress field ahead of the crack tip is sufficiently high to cause debonding of the nanofillers from the epoxy, and so enables subsequent plastic void growth in the epoxy polymer. (The elastic modulus of the nanofillers is much higher than that of the epoxy matrix, and consequently a localised stress concentration is generated at the nanofiller-epoxy interface that leads to the interfacial debonding and subsequent void formation in the epoxy.) These voids are indicative of plastic deformation of the epoxy polymer in the process zone. Thus, a relatively large amount of plastic energy is dissipated via growth of the voids and this may significantly contribute to increasing the fracture energy of the epoxy nanocomposites. The volume content of the voids increased with increasing nanofiller concentration. This accounts, in part, for the increased fracture energy of the nanocomposites with increasing CNF or GNP content, as discussed in detail below.

In addition to the intrinsic toughening processes discussed above, several extrinsic toughening mechanisms operating behind the crack front were observed in the epoxy nanocomposites, and these mechanisms were not present in the unmodified epoxy polymer. As noted above, intrinsic toughening mechanisms operate ahead of the main crack front and they included (i) debonding of the nanofiller, (ii)

epoxy void growth and (iii) micro-cracking, as shown schematically in **Fig. 5**. While extrinsic toughening mechanisms operate behind the crack front and involved (i) pull-out, (ii) crack bridging and (iii) rupture of the nanofillers, again as shown schematically in **Fig. 5**. **Fig. 6a-b** shows the formation of a crack bridging zone by the CNFs and the GNPs, which results from their interfacial debonding and pull-out from the epoxy. As the crack front passes across the nanofillers, they start to debond and pull-out from the fracture surface containing the shorter embedded lengths, which leads to the formation of the crack bridging zone. These extrinsic toughening mechanisms shield the crack tip from the applied stress and thereby increases the fracture energy. However, any relatively long nanofillers rupture close to the crack plane, since their embedded length is sufficiently long to prevent debonding, thereby causing them to rupture rather than pull-out. The fraction of nanofillers encountered by the crack front increases with increasing nanofiller concentration. This therefore contributes to the increased fracture energy of the nanocomposites that was measured with an increasing concentration of the CNF or the GNP nanofillers.

3.3 Fracture energy modelling

The recorded improvements in the fracture energy of the epoxy were due to the energy dissipated from the following major toughening mechanisms: (a) debonding of the nanofillers, ΔG_{db}, (b) plastic void growth of the epoxy polymer initiated by the debonded nanofillers in the process zone ahead of the crack tip, ΔG_v, (c) pull-out of the nanofillers bridging the crack, $\Delta G_{pull-out}$, and (d) rupture of the nanofillers behind the crack tip, $\Delta G_{rupture}$. A method for estimating the fracture energy contribution from each of these primary toughening mechanisms was presented in our previous studies by considering the conventional theories for fibre reinforcement by CNFs [9] and platelets for GNPs [35].

By combining the energy dissipated via each of the toughening mechanisms, the fracture energy, G_{Ic}, of the epoxy nanocomposites containing the 1-D or 2-D nanofillers can be calculated from the following expressions:

$$G_{Ic} = G_{CU} + \Delta G_{pull-out} + \Delta G_{rupture} + \Delta G_{db} + \Delta G_v \quad (1)$$

Thus, we have from [9,27,35]:

(a) For the CNF-epoxy nanocomposites:

$$G_{Ic,CNF} = G_{CU} + \frac{V_f \sigma_f^2 d_f}{8\tau_i} + \frac{V_f \sigma_f^2 l_f}{2 E_f} + \frac{V_f l_{po} G_i}{d_f} + \left(1 + \frac{\mu_m}{\sqrt{3}}\right)^2 V_f \left(\frac{d_v^2}{3 d_f^2} + \frac{d_v}{3 d_f} - \frac{2}{3}\right) \sigma_y r_{yu} K_{vm}^2 \quad (2)$$

(b) For the GNP-epoxy nanocomposites:

$$G_{Ic,GNP} = G_{CU} + \frac{V_f\, t\, W\, \sigma^2}{2\,(t+W)\,\tau_G} + \frac{V_f\, l\, \sigma^2}{2\, E_G} + \frac{2 V_f\,(t+W)\, l_{po}\, G_i}{t\, W} + \left(1 + \frac{\mu_m}{\sqrt{3}}\right)^2 [V_{void} - V_f] \sigma_y r_{yu} K_{vm}^2 \quad (3)$$

(c) Therefore, for the hybrid-epoxy nanocomposites:

$$G_{Ic,Hybrid} = V_{f,CNF}\,(G_{Ic,CNF}) + V_{f,GNP}\,(G_{Ic,CNF}) \quad (4)$$

The definition of the parameters in Eqs. 2-4 and their values are given in Table 1. The term V_f is the volume fraction of the carbon nanofiller. For the CNF-epoxy nanocomposites, the voids were assumed to be a truncated cone in shape with a diameter on the fracture surface of d_v. The average value of d_v for the epoxy-CNF nanocomposites and of the volume fraction of the voids, V_{void}, around the GNPs were measured using scanning electron microscopy. The pull-out length, l_{po}, of the nanofillers was taken to be equal to half their length.

A comparison of the predictions from the above theoretical models with the experimentally measured values of the fracture energies for the three types of epoxy nanocomposites is shown in **Fig. 7**. As may be seen, there is good agreement between the predictions and the measured values of G_{Ic}, until the highest concentration of the nanofillers was employed when agglomeration of the nanofillers was observed, which is not taken in into account in the modelling studies. Thus, the results shown in **Fig. 7** confirm that the primary toughening mechanisms, described in above Eqs. 2-4 for the epoxy nanocomposites modified using the CNFs or the GNPs or the hybrid nanofillers, were the main operative mechanisms. Further, good agreement exists between the experimental results and the calculated fracture energies for the additive model that was proposed for the hybrid nanocomposites. Thus, for the hybrid nanocomposites, the separate toughening contributions from the two nanofillers may be simply summed. Therefore, no significant interactions appear to occur between the two nanofillers with respect to the toughening mechanisms, which would have resulted in synergistic toughening effects being observed for the hybrid nanocomposites.

Further, the calculated contributions to the improvement in the fracture energy, G_{Ic}, from each of the above toughening mechanisms are given in Table 2. Nanofiller pull-out and void growth are the two most dominant toughening mechanisms, accounting for the majority of the fracture energy enhancement for all three types of nanocomposites. A notable difference between the modelling results for the nanocomposites was that the intrinsic toughening due to void growth was far more pronounced in the CNF-epoxy nanocomposites. Indeed, it is this aspect that leads to the CNFs being significantly more effective at increasing the toughness, G_{Ic}, of the epoxy compared to the GNPs.

4. Results and discussion: Cyclic fatigue behaviour of the epoxy nanocomposites

4.1 Cyclic fatigue measurements

Fig. 8 shows the logarithmetic fatigue crack growth rate, *da/dN*, curves against the logarithmetic square-root of the maximum energy release-rate in a given cycle, $\sqrt{G_{max}}$, for the unmodified epoxy and the epoxy nanocomposites. It should be noted that, for polymeric adhesive layers (see **Fig. 1**), and for fibre-reinforced polymers, the energy release-rate, *G*, approach, rather than the stress-intensity factor, *K*, approach, is invariably used to study crack growth and delamination growth in such materials [29,42-44]. Thus, by analogy with the extensive work [45-47] of Paris and others on metals, where the range, ΔK, of the applied stress-intensity factor is employed to analyse the data, at first sight the most obvious and corresponding parameter against which to plot the measured rate of the fatigue crack growth, *da/dN*, for such polymeric-based materials is the range of the applied energy release-rate, ΔG, where $\Delta G = G_{max} - G_{min}$. However, since *K* is proportional to $\sqrt{G}$, experimental and theoretical work has demonstrated [48-53] that the logical extension of the Paris fatigue crack growth equation for metals to fatigue cracking in such polymeric materials is, in fact, to express *da/dN* as a function of $\Delta\sqrt{G}$, or $\sqrt{G_{max}}$, rather than ΔG, or G_{max}; where $\Delta\sqrt{G}$ is given by $\Delta\sqrt{G} = (\sqrt{G_{max}} - \sqrt{G_{min}})$. In the present work, in accord with these previous studies, the parameter $\sqrt{G_{max}}$ has been employed.

The plots of the measured crack growth rate, *da/dN* versus $\sqrt{G_{max}}$ are shown in **Fig. 8** and they exhibit the typical relationship expected, with three distinct regions of fatigue crack growth. Namely, Region 1: a threshold region with very slow, or no, fatigue crack growth which corresponds to attaining the

value of the threshold energy-release rate, $\sqrt{G_{th}}$; Region 2: a steady-state, linear fatigue crack growth region which follows the Paris equation; and Region 3: an unstable (rapid) fatigue crack growth region which leads to the quasi-static fracture energy, G_{Ic}. The value of the threshold energy release-rate was taken at 10^{-9} m/cycle, which is very close to the lowest value of *da/dN* that could be reliably measured in the fatigue tests.

There is a major improvement in the cyclic fatigue resistance for the epoxy nanocomposites, even though the weight fractions of the nanofillers are relatively low. The fatigue crack growth rate curves for the epoxy nanocomposites in **Fig. 8** are further to the right-hand side of the graph compared with the unmodified epoxy. Thereby showing that the rate of fatigue crack growth for the epoxy nanocomposites are much lower than that for the unmodified epoxy, at a given value of $\sqrt{G_{max}}$. The resistance to fatigue crack growth also increases with an increasing concentration of the nanofillers. As reported above for the quasi-static fracture energy, G_{Ic}, this was due to a greater extent of the toughening mechanisms being induced by the nanofillers as their concentration was increased. The threshold value of the maximum energy-release rate, $\sqrt{G_{th}}$, below which no significant fatigue crack growth occurs, was similar in value for the same concentration of CNF or GNP in the epoxy nanocomposites. Indeed, the epoxy nanocomposites containing either the CNF or the GNP exhibit similar fatigue resistance in the near-threshold region, i.e. below crack growth rates, *da/dN*, of ~10^{-7} m/cycle, for a given concentration of nanofiller.

4.2 Fatigue toughening mechanisms

The improvement to the fatigue resistance of the epoxy nanocomposites was due to a range of toughening mechanisms induced by the carbon nanofillers which were operative under cyclic loading. Similar to the case of quasi-static loading described above, a combination of intrinsic and extrinsic toughening mechanisms were operative under cyclic loading. These mechanisms were (a) debonding of the nanofillers, (b) plastic void growth initiated by the debonded nanofillers in the process zone ahead of the crack tip, (c) crack bridging and pull-out of the nanofillers behind the crack tip; and (d) rupture of the nanofillers behind the crack tip. However, under fatigue loading, the nanofillers induced additional toughening mechanisms which were not evident under quasi-static loading, as shown in **Fig. 9**. For example, in **Fig. 9a**, a small

fraction of the CNFs have undergone an unravelling deformation mechanism under cyclic loading, and this has not been observed under quasi-static loading. Under cyclic loading, the outer layer of the CNFs tended to fail prior to the unravelling of the inner helical core (see **Fig. 9b**). This was due to the fact that, during fatigue loading, the CNFs within the crack-bridging zone experience, sequentially, cyclic-tension and cyclic-compression loading, which causes progressive failure of the outer layer and subsequent incremental unravelling of the inner core of the CNF. However, despite the damage to the outer layer, the unravelling of the inner core of the CNFs continues to allow the crack-bridging mechanism to operate, as shown in **Fig. 9c**, thereby contributing to the improved fatigue performance.

In contrast, fractographic examination of the GNP-epoxy nanocomposites revealed the presence of debris particles along the fatigue crack, as shown for example in **Fig. 9d.** Such particles are formed due to the crack tip branching that occurred within the process zone of the GNP nanocomposites. As can be seen in **Fig. 3e**, at the location of a branching crack tip, the fracture planes overlap before they coalesce into a single main crack. This produces a scarp, or cleavage, step along the fracture surface and causes the formation of partly detached fragments along the wake of the crack, as shown in **Fig. 10a-b**. Indeed, Purslow [54] has described the origin and development of similar features for various epoxy-based composite materials. Under the cyclic loading, these fragments break and become wedged between the fatigue crack surfaces. Such debris particles can induce toughening by shielding the crack tip, particularly when the crack opening is small, i.e. less than the particle size [55]. Thus, in the near threshold region, where the crack opening/closing displacements within a load cycle are relatively very small (i.e. as $G_{max} \rightarrow G_{th}$), the debris particles (which are larger than the displacements) induce a crack shielding effect which retards the fatigue crack growth, at a given $\sqrt{G_{max}}$ value.

4.3 Comparison of quasi-static fracture energy and cyclic fatigue properties

Fig. 11a shows the measured relationship between the values of the fatigue threshold fracture energy, G_{th}, and the quasi-static fracture energy, G_{Ic}, for the epoxy nanocomposites. Also included are results taken from Kinloch et. al. [56] for a different unmodified epoxy to that used in the present work with a higher fracture energy value, G_{Ic}, of 495 J/m^2. This epoxy was modified with a wide range of polymeric-based

tougheners, and the results are shown in **Fig. 11** for the unmodified (i.e. neat) epoxy and when modified with: (a) 10 wt% of a difunctional epoxydised polysulfide (10PS), (b) 10 wt% of core-shell rubber particles (consisting of a polybutadiene core with a functionalised poly(methyl methacrylate) shell) (10CSi), and (c) 10 wt% of a poly(propylene glycol)-based polyurethane (10PU). (These particular tougheners and concentrations were selected from [56] on the basis that they represent the least effective, an intermediately effective and the most effective tougheners in terms of increasing the value of G_{Ic}.)

There are several interesting features revealed by the plot in **Fig. 11a**. Firstly, the threshold G_{th} values determined from the cyclic fatigue tests are significantly lower than the corresponding quasi-static fracture energy, G_{Ic}, values. This, of course, simply illustrates the well-established fact that cyclic-fatigue loading is far more damaging to a material than quasi-static loading. Indeed, it is noteworthy that most of the results, especially for the epoxies with a relatively high quasi-static toughness, fall on (or below) a line representing $G_{th}/G_{Ic} = 0.1$. Secondly, values of the carbon nanofillers used in the present study are not as effective at increasing the absolute value of G_{Ic} as the CSi and PU polymeric tougheners. Thirdly, however, it should be noted that the toughness of the unmodified epoxy employed in [56] was significantly tougher than that used in the present study, again see **Fig. 11a**.

Indeed, when the toughnesses of the epoxy nanocomposites and those modified using the polymeric tougheners are normalised with respect to the G_{Ic} value for the respective unmodified epoxy, then the results for the present epoxy nanocomposites are shown to give better improvements in toughness compared to the epoxy modified using the polymeric tougheners [56], see **Fig. 11b**. A similar finding emerges with respect to the fatigue threshold values, G_{th}, determined from the cyclic-fatigue tests. The results in **Fig. 11b** show that at a low concentration (i.e. 0.5 wt%) of nanofillers then the normalised ratio, G_{th}/G_{Ic}, for the epoxy nanocomposites is ~1:1, which reveals an equal level of improvement in the values of the fatigue threshold and the fracture energy. However, at higher concentrations of the CNFs or the GNPs, the ratio G_{th}/G_{Ic} falls below 1:1, thereby indicating a lower efficacy at improving the threshold fracture energy, G_{th}, compared with the quasi-static fracture energy, G_{Ic}, of the unmodified epoxy; and this effect is more pronounced for the epoxy-CNF nanocomposite than for the epoxy-GNP nanocomposite. It is also of interest that the results for the epoxy nanocomposites containing 1.0 wt% of either CNFs or GNPs give

higher values of the normalised ratio, G_{th}/G_{Ic}, for than for the epoxy modified with the polymeric tougheners.

The above behaviour of the various epoxies arises from the dynamic relationship between the stress-state ahead of the crack tip and the extent of the intrinsic toughening mechanisms, most notably the plastic void growth mechanism, that operates within the process zone. The radius of the process zone, r_{yu}, is given by [51]:

$$r_{yu} = \frac{1}{6\pi}\left(\frac{E\,G_{max}}{\sigma_y^2}\right) \quad (5)$$

where E is the Young's modulus of the epoxy and G_{max} is the maximum applied energy release-rate. Thus, for relatively low values of $\sqrt{G_{max}}$ in the fatigue cycle the size of the process zone ahead of the crack tip becomes relatively very small, as shown schematically in **Fig. 12**. Indeed, this process zone may be so small in size that it only contains a few nanofiller (or polymeric toughener) particles that can initiate any intrinsic toughening mechanisms. This will, of course, greatly reduce the contributions from the debonding and void growth toughening mechanisms as the value of $\sqrt{G_{max}}$ decreases and tends towards the very low value of the threshold. Now, from **Table 2**, the modelling studies reveal that the toughening due to plastic void growth is more dominant in the CNF-epoxy nanocomposites than for the GNP-epoxy nanocomposites. Thus, as indeed observed, the CNF nanocomposites would be expected to experience a relatively greater reduction in toughening from debonding and void growth processes due to the reduction in the process zone size when, in the fatigue tests, the threshold energy-release rate, G_{th}, is approached. Similarly, the 10CSi modified epoxy polymer, which also largely derives its relatively high toughness from promoting plastic void growth in the process zone [56], again possesses a relatively low value of the ratio G_{th}/G_{Ic}. Indeed, Kinloch et al. [56] reported that, for this 10CSi-modified epoxy polymer, the plastic void growth mechanism was found to be operative under quasi-static loading but not under cyclic fatigue loading.

Finally, on the other hand, the unravelling of the CNFs observed under cyclic fatigue loading will improve the fatigue performance of the CNF-epoxy nanocomposites. Indeed, molecular-dynamic simulations have shown that the unravelling of the CNFs can dissipate significant energy due to the

breaking of the secondary bonds within the inner helical core [57,58]. Also, although the GNP-epoxy nanocomposites will also experience similar process-zone size effects as the value of G_{th} is approached, the additional toughening due to the crack wedging mechanism will mitigate these effects to some degree. Thus, the presence of these extrinsic toughening mechanisms, which only operate in the epoxy nanocomposites, mitigates the effects of a decrease in the extent of the intrinsic toughening mechanisms as the value of G_{th} is approached. Therefore, as shown in **Fig. 11b,** the superior improvement in the overall resistance to fatigue cracking near the threshold region for the epoxy nanocomposites, compared with the epoxies modified using the polymeric tougheners (relative to their corresponding unmodified epoxy) arises from the fact that the latter do not exhibit any extrinsic toughening mechanisms.

5. Conclusions

The effects of the shape and concentration of nanoscale carbon fillers on the quasi-static fracture energy and cyclic-fatigue crack growth resistance of epoxy nanocomposites have been investigated. The improvement to the mode I fracture energy, G_{Ic}, and the fatigue properties of the nanocomposites were due to the toughening mechanisms induced by the 1-D CNFs or 2-D GNPs via a combination of intrinsic and extrinsic toughening mechanisms including (a) debonding of the nanofillers, (b) plastic void growth initiated by the debonded nanofillers, (c) pull-out and crack bridging of the nanofillers; and (d) rupture of the bridging nanofillers. In addition, the cyclic-fatigue loading of the epoxy nanocomposites induced additional extrinsic mechanisms including (a) unravelling of the inner helical core of the CNFs and (b) crack wedging from the debris formed due to the microcracking induced by the GNPs.

The results from modelling the primary toughening mechanisms that were identified demonstrated that the predicted values of the fracture energy, G_{Ic}, associated with such mechanisms were in good agreement with the experimental results. Further, the model results revealed that the 1-D CNFs and 2-D GNPs were approximately equally effective at improving the extrinsic toughness via crack bridging and pull-out. However, the CNFs were very significantly more effective than the GNPs at increasing the intrinsic toughening effect associated with the plastic void growth of the epoxy polymer. Thus, overall, the CNFs were more effective at increasing the toughness, G_{Ic}, of the epoxy polymer compared with the GNPs. Further, the improvements in the measured values of the fracture energy from the presence of the both the

CNFs and the GNPs in the hybrid-epoxy nanocomposites were equivalent to the sum of the separate toughening contributions from the two respective nanofillers. The measured values of G_{Ic} for the hybrid nanocomposites were also in good agreement with the proposed additive toughening model. These observations revealed that there were no synergistic toughening mechanisms which were operative between the two nanofillers in these epoxy nanocomposites.

The addition of CNFs or GNPs to the epoxy was also effective at promoting the fatigue crack growth resistance near the threshold region. However, the CNFs were more efficient than the GNPs at resisting the rapid fatigue crack growth that occurred at higher values of the cyclic energy release-rate, i.e. as the value of the quasi-static fracture energy, G_{Ic}, of the nanocomposites was approached. The improvements in the values of the fatigue threshold energy, G_{th}, necessary to initiate fatigue cracking in both nanocomposites containing 1.0 wt% of CNFs or GNPs were relatively low compared with the improvements in the quasi-static fracture energy G_{Ic}. This was due to a decrease in the energy dissipated via the intrinsic toughening processes, such as the void growth mechanism, under cyclic-fatigue loading. This was suggested to arise from the relatively very small size of the process zone ahead of the crack tip, which results at very low values of applied energy release-rate, i.e. as the fatigue threshold value, G_{th}, is approached. However, the presence of extrinsic toughening mechanisms in these epoxy nanocomposites did mitigate, to some degree, the effects of this decrease in the effectiveness of the intrinsic toughening mechanisms as the fatigue threshold value, G_{th}, was approached.

Finally, a comparison of the fracture and fatigue properties of the epoxy nanocomposites with previous literature on polymeric-based toughening agents for epoxies has shown that the present nanoscale carbon fillers are very effective at improving both the fracture and fatigue performance of an epoxy. Further, such carbon nanofillers may also, of course, offer other improved multifunctional properties such as electrical conductivity and damage-sensing capabilities [5,28].

Acknowledgements

The authors are grateful for the financial support received from the Australian Research Council's Discovery Grant Program (DP140100778).

References

[1] Young RJ, Kinloch IA, Gong L, Novoselov, KS. The mechanics of graphene composites: A review. Composites Science and Technology. 2012;72:1459-76.

[2] Zhang J, Terrones M, Park RC, Mukherjee R, Monthioux M, Koratkar N. et al. Carbon Science in 2016: Status, challenges and perspectives. Carbon. 2016;98:708-32.

[3] Ahmadi-Moghadam B, Sharafimasooleh M, Shadlou S, Taheri F. Effect of functionalization of graphene nanoplatelets on the mechanical response of graphene/epoxy composites. Materials & Design. 2015;66:142-9.

[4] Rafiee MA, Rafiee J, Srivastava I, Wang Z, Song H, Yu ZZ, Koratkar N. Fracture and fatigue in graphene nanocomposites. Small. 2010;6:179-83.

[5] Wu S, Ladani RB, Zhang J, Bafekrpour E, Ghorbani K, Mouritz AP, Kinloch AJ, Wang CH. Aligning multilayer graphene flakes with an external electric field to improve multifunctional properties of epoxy nanocomposites. Carbon. 2015;94:607-18.

[6] Ayatollahi MR, Shadlou S, Shokrieh MM. Fracture toughness of epoxy/multi-walled carbon nanotube nano-composites under bending and shear loading conditions. Materials & Design. 2011;32:2115-24.

[7] Hadavand BS, Javid KM, Gharagozlou M. Mechanical properties of multi-walled carbon nanotube/epoxy polysulfide nanocomposite. Materials & Design. 2013;50:62-7.

[8] Bal S. Experimental study of mechanical and electrical properties of carbon nanofiber/epoxy composites. Materials & Design. 2010;31:2406-13.

[9] Ladani RB, Wu S, Kinloch AJ, Ghorbani K, Zhang J, Mouritz AP, Wang CH. Improving the toughness and electrical conductivity of epoxy nanocomposites by using aligned carbon nanofibres. Composites Science and Technology. 2015;117:146-58.

[10] Wu S, Ladani RB, Zhang J, Kinloch AJ, Zhao Z, Ma J, Zhang X, Mouritz AP, Ghorbani K, Wang CH. Epoxy nanocomposites containing magnetite-carbon nanofibers aligned using a weak magnetic field. Polymer. 2015;68:25-34.

[11] Bortz DR, Heras EG, Martin-Gullon I. Impressive fatigue life and fracture toughness improvements in graphene oxide/epoxy composites. Macromolecules. 2012;45:238-45.

[12] Esawi AMK, Farag MM. Carbon nanotube reinforced composites: Potential and current challenges. Materials & Design. 2007;28:2394-401.

[13] Hadden CM, Klimek-McDonald DR, Pineda EJ, King JA, Reichanadter AM, Miskioglu I, Gowtham S, Odegard GM. Mechanical properties of graphene nanoplatelet/carbon fiber/epoxy hybrid composites: Multiscale modeling and experiments. Carbon. 2015;95:100-12.

[14] Hamer S, Leibovich H, Green A, Avrahami R, Zussman E, Siegmann A, Sherman D. Mode I and Mode II fracture energy of MWCNT reinforced nanofibrilmats interleaved carbon/epoxy laminates. Composites Science and Technology. 2014;90:48-56.

[15] Li J, Wong P-S, Kim J-K. Hybrid nanocomposites containing carbon nanotubes and graphite nanoplatelets. Materials Science and Engineering: A. 2008;483-484:660-3.

[16] Yang S-Y, Lin W-N, Huang Y-L, Tien H-W, Wang J-Y, Ma C-CM, Li S-M, Wang Y-S. Synergetic effects of graphene platelets and carbon nanotubes on the mechanical and thermal properties of epoxy composites. Carbon. 2011;49:793-803.

[17] Wang J, Jin X, Wu H, Guo S. Polyimide reinforced with hybrid graphene oxide @ carbon nanotube: Toward high strength, toughness, electrical conductivity. Carbon. 2017;123:502-13.

[18] Li W, Dichiara A, Bai J. Carbon nanotube–graphene nanoplatelet hybrids as high-performance multifunctional reinforcements in epoxy composites. Composites Science and Technology. 2013;74:221-7.

[19] Li Y, Wang S, Wang Q, Xing M. A comparison study on mechanical properties of polymer composites reinforced by carbon nanotubes and graphene sheet. Composites Part B: Engineering. 2018;133:35-41.

[20] Ahmadi-Moghadam B, Taheri F. Fracture and toughening mechanisms of GNP-based nanocomposites in modes I and II fracture. Engineering Fracture Mechanics. 2014;131:329-39.

[21] Domun N, Paton KR, Hadavinia H, Sainsbury T, Zhang T, Mohamud H. Enhancement of fracture toughness of epoxy nanocomposites by combining nanotubes and nanosheets as fillers. Materials. 2017;10:1179-97.

[22] Zhang G, Karger-Kocsis J, Zou J. Synergetic effect of carbon nanofibers and short carbon fibers on the mechanical and fracture properties of epoxy resin. Carbon. 2010;48:4289-300.

[23] Chatterjee S, Nafezarefi F, Tai NH, Schlagenhauf L, Nüesch FA, Chu BTT. Size and synergy effects of nanofiller hybrids including graphene nanoplatelets and carbon nanotubes in mechanical properties of epoxy composites. Carbon. 2012;50:5380-6.

[24] Jones R, Pitt S, Hui D, Brunner A. Fatigue crack growth in nano-composites. Composite Structures. 2013;99:375-9.

[25] Ladani RB, Ravindran AR, Wu S, Pingkarawat K, Kinloch AJ, Mouritz AP, Ritchie RO, Wang CH. Multi-scale toughening of fibre composites using carbon nanofibres and z-pins. Composites Science and Technology. 2016;131:98-109.

[26] Zhang W, Picu RC, Koratkar N. The effect of carbon nanotube dimensions and dispersion on the fatigue behavior of epoxy nanocomposites. Nanotechnology. 2008;19:285709, 1-5.

[27] Hsieh TH, Kinloch AJ, Taylor AC, Kinloch IA. The effect of carbon nanotubes on the fracture toughness and fatigue performance of a thermosetting epoxy polym. Journal of Materials Science. 2011;46(23):7525-35.

[28] Ladani RB, Wu S, Kinloch AJ, Ghorbani K, Mouritz AP, Wang CH. Enhancing fatigue resistance and damage characterisation in adhesively-bonded composite joints by carbon nanofibres. Composites Science and Technology. 2017;149:116-26.

[29] ISO-25217. Determination of the mode I adhesive fracture energy of structural adhesive joints using double cantilever beam and tapered double cantilever beam specimens. Geneva, Switzerland. 2009.

[30] ASTM-E647. Standard test method for measurement of fatigue crack growth rates. ASTM International; 2015.

[31] Ritchie RO. Mechanisms of fatigue-crack propagation in ductile and brittle solids. International Journal of Fatigue. 1999;100:55-83.

[32] Lawrence JG, Berhan LM, Nadarajah A. Elastic properties and morphology of individual carbon nanofibers. ACS Nano. 2008;2:1230-6.

[33] Ramos A, Cameán I, García AB. Graphitization thermal treatment of carbon nanofibers. Carbon. 2013;59:2-32.

[34] Nirmalendran S., Horii H. Analytical modeling of microcracking and bridging in the fracture of quasi-static materials. Journal of Mechanics and Physics of Solids. 1992;40:863-86.

[35] Ladani RB, Wu S, Kinloch AJ, Ghorbani K, Zhang J, Mouritz AP, Wang CH. Multifunctional properties of epoxy nanocomposites reinforced by aligned nanoscale carbon. Materials & Design. 2016;94:554-64.

[36] SIGMA-ALDRICH. Properties and application of carbon nanofibers (CNFs) synthesized using vapor grown carbon fiber (VGCF) manufacturing technology http://www.sigmaaldrich.com/china-mainland/zh/materials-science/nanomaterials/carbon-nanofibers.html. 2015.

[37] XG-Sciences. xGnP Grade M Product Characteristics. http://xgsciencescom/wp-content/uploads/2012/10/10-15-13_xGnP-M_Data-Sheetpdf. 2015.

[38] Ozkan T, Naraghi M, Chasiotis I. Mechanical properties of vapor grown carbon nanofibers. Carbon. 2010;48(1):239-44.

[39] Westsystem. 105 resin engineering data http://www.westsystem.com/ss/assets/Product-Data-PDFs/TDS%20105_206.pdf. 2015.

[40] Gong L, Kinloch IA, Young RJ, Riaz I, Jalil R, Novoselov KS. Interfacial stress transfer in a graphene monolayer nanocomposite. Advanced Materials. 2010;22:2694-97.

[41] Huang Y, Kinloch AJ. Modelling of the toughening mechanisms in rubber-modified epoxy polymers. 2. A quantitative description of the microstructure fracture property relationships. Journal of Materials Science. 1992;27:2763-9.

[42] Wang SS, Mandell JF, McGarry J. Analysis of crack tip stress-field in DCB adhesive fracture specimens. International Journal of Fracture. 1978;14;39-58.

[43] Tvergaard V, Hutchinson JW. The influence of plasticity on mixed mode interface toughness. Journal Mechanics and Physics of Solids.1993; 41:1119-35.

[44] ISO-15024. Fibre-reinforced plastic composites -Determination of mode I interlaminar fracture toughness, GIC, for unidirectionally reinforced materials. Geneva, Switzerland. 2001.

[45] Paris PC, Gomez RE, Anderson WE. A rational analytic theory of fatigue. The Trend in Engineering.1961;13: 9-14.

[46] Paris PC, Erdogan F. Critical analysis of crack growth propagation laws. ASME Transactions Journal Basic Engineering. 1963;85D:528-34.

[47] Paris PC. A brief history of the crack tip stress intensity factor and its application. Meccanica, 2014:49:759–64.

[48] Sih GC, Paris PC, Irwin GR. On cracks in rectilinearly anisotropic bodies. International Journal of Fracture Mechanics. 1965; 1:189-203.

[49] Rans C, Alderliesten R, Benedictus R. Misinterpreting the results: How similitude can improve our understanding of fatigue delamination growth. Composites Science and Technology. 2011; 71: 230-38.

[50] Jones R, Hu W, Kinloch AJ. A convenient way to represent fatigue crack growth in structural adhesives. Fatigue and Fracture of Engineering Materials & Structures. 2015;38:379-91.

[51] Donough MJ, Gunnion AJ, Orifici AC, Wang CH. Scaling parameter for fatigue delamination growth in composites under varying load ratios. Composites Science and Technology. 2015;120:39-48.

[52] Jones R., Kinloch AJ., Hu W., (2016) Cyclic-FCG in composite and adhesively-bonded structures: the FAA slow crack growth approach to certification and the problem of similitude. International Journal of Fatigue. 2016;88:10-8.

[53] Jones R, Kinloch AJ, Michopoulos JG, Brunner AJ, Phan N. Delamination growth in polymer-matrix fibre composites and the use of fracture mechanics data for material characterisation and life prediction. Composite Structures. 2017; 180:316-33.

[54] Purslow D. Matrix fractography of fibre-reinforced epoxy composites. Composites. 1986;17:289-303.

[55] Ritchie RO. Mechanisms of fatigue crack propagation in metals, ceramics and composites: Role of crack tip shielding. Materials Science and Engineering: A. 1988;103:15-28.

[56] Kinloch AJ, Lee SH, Taylor AC. Improving the fracture toughness and the cyclic-fatigue resistance of epoxy-polymer blends. Polymer. 2014;55:6325-34.

[57] Gu J, Sansoz F. An atomistic simulation study of the mechanisms and kinetics of surface bond strengthening in thermally-treated cone-stacked carbon nanofibers. Carbon. 2013;56:351-7.

[58] Gu J, Sansoz F. Superplastic deformation and energy dissipation mechanism in surface-bonded carbon nanofibers. Computational Materials Science. 2015;99:190-4.

Figures and Tables

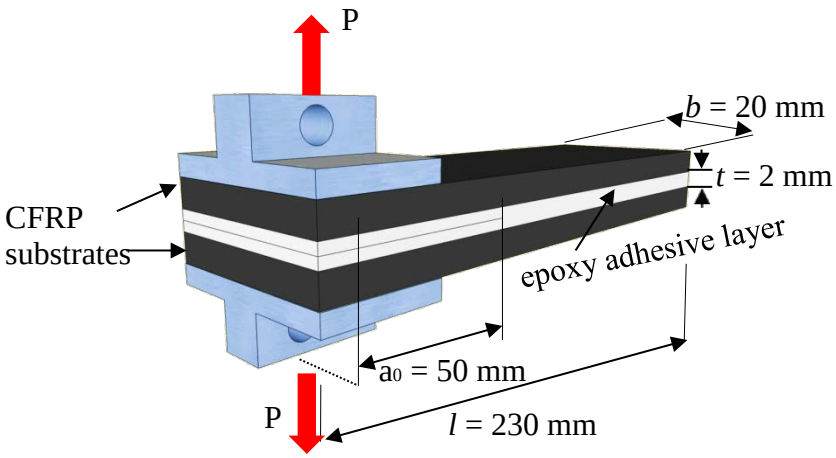

Fig 1. Schematic diagram of the double cantilever beam (DCB) specimen used for the fracture energy and cyclic-fatigue testing.

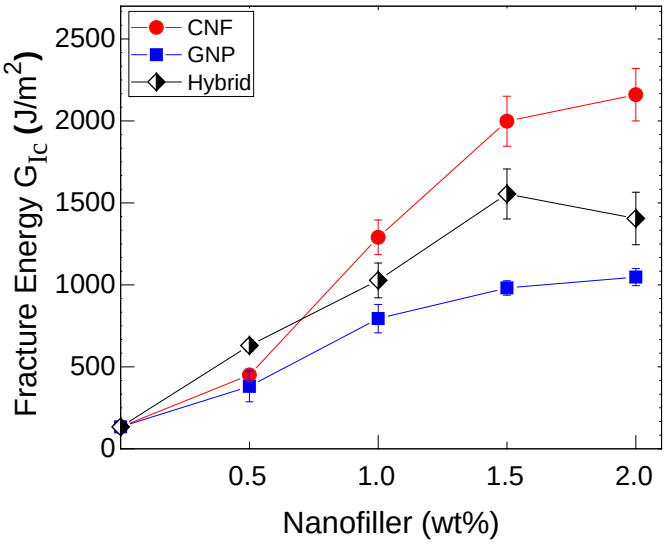

Fig 2. Effects of the type and concentration of nanofiller on the fracture energy of the epoxy nanocomposites. (Note: The hybrid nanofiller wt% consists of 50% of each of the nanofiller types. The error bars represent ± one standard deviation.)

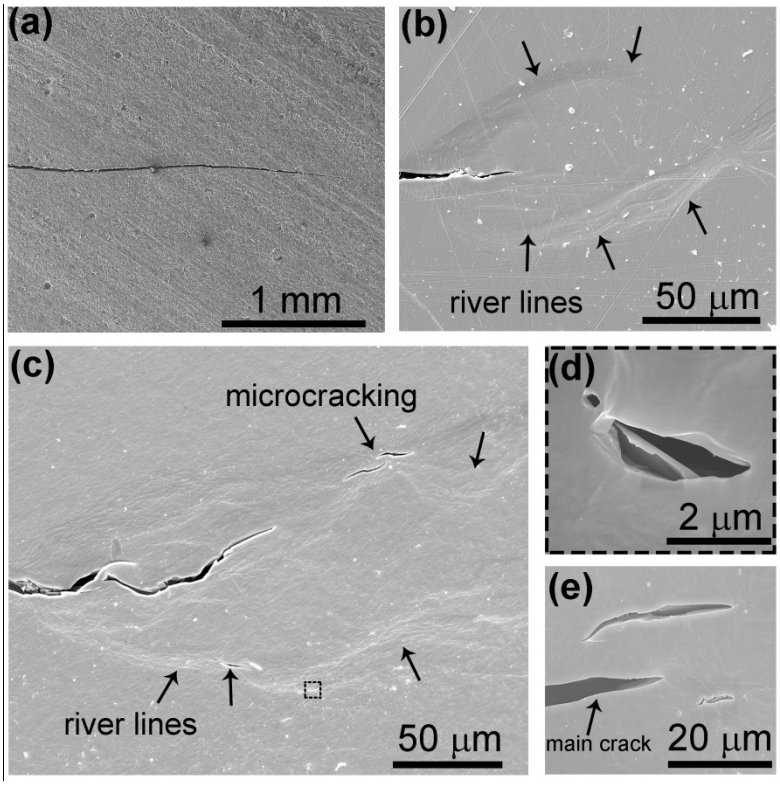

Fig. 3 SEM images of the side-view at crack tip region of the (a) unmodified epoxy; (b) an epoxy nanocomposite containing 1.0 wt% CNFs; and (c-e) an epoxy nanocomposite containing 1.0 wt% GNPs. (The direction of crack growth is from left to right. The box in image (c) indicates the location where the image shown in (d) was taken.)

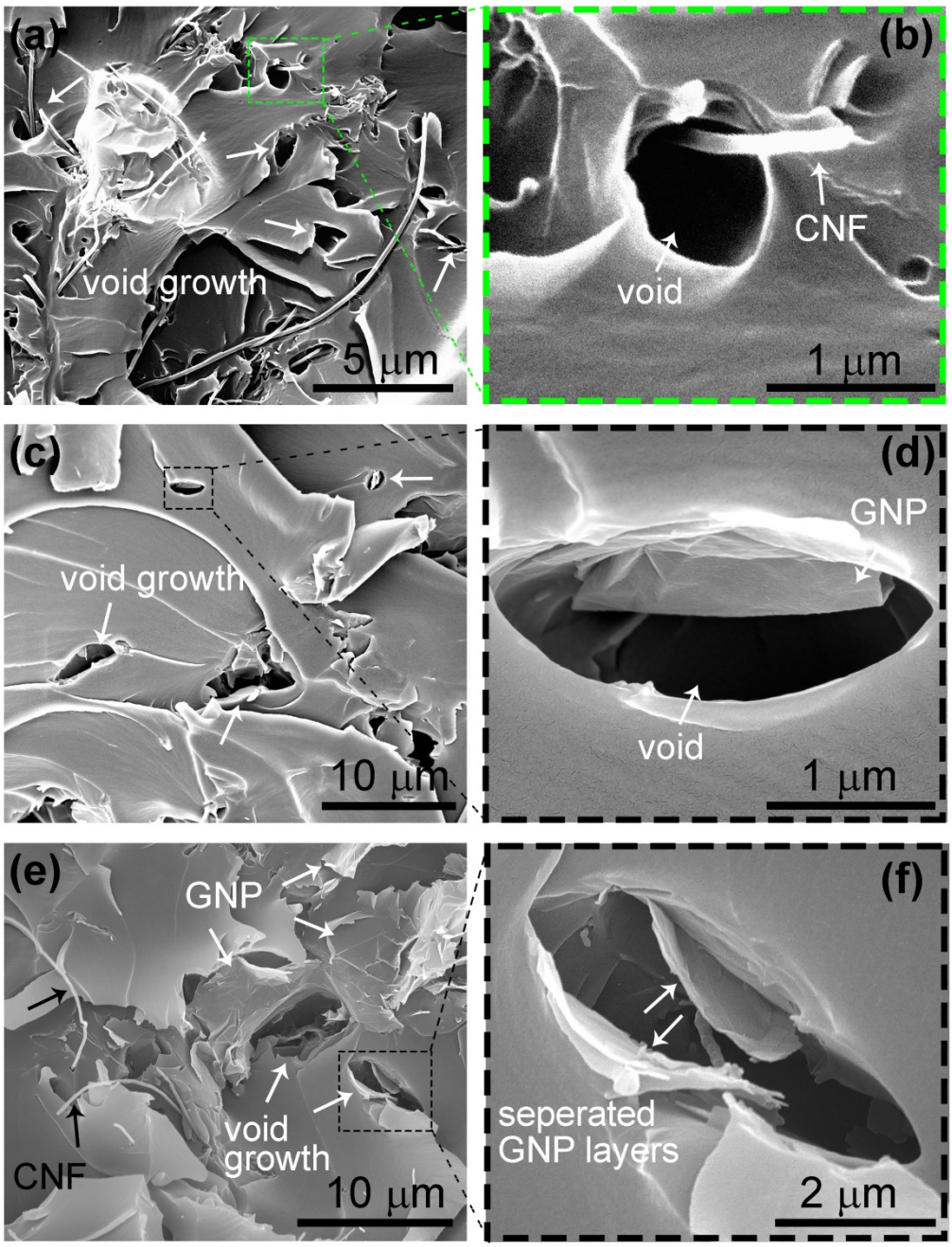

Fig. 4 Representative SEM images of the fracture surfaces of the region immediately ahead of the crack tip of the epoxy nanocomposites containing: (a-b) 1.0 wt% CNFs, (c-d) 1.0 wt% GNPs and (e-f) 0.5 wt% CNF + 0.5 wt% GNP.

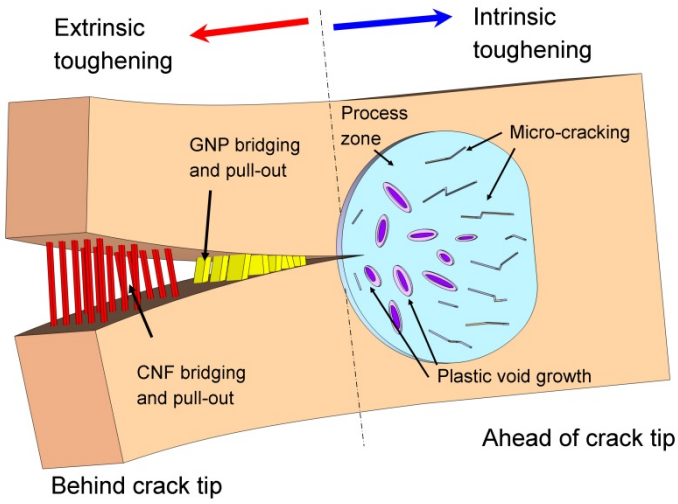

Fig. 5 A schematic representation of the intrinsic and extrinsic toughening mechanisms observed in the epoxy nanocomposites. (The positions of the CNFs and GNPs are idealised for clarity.)

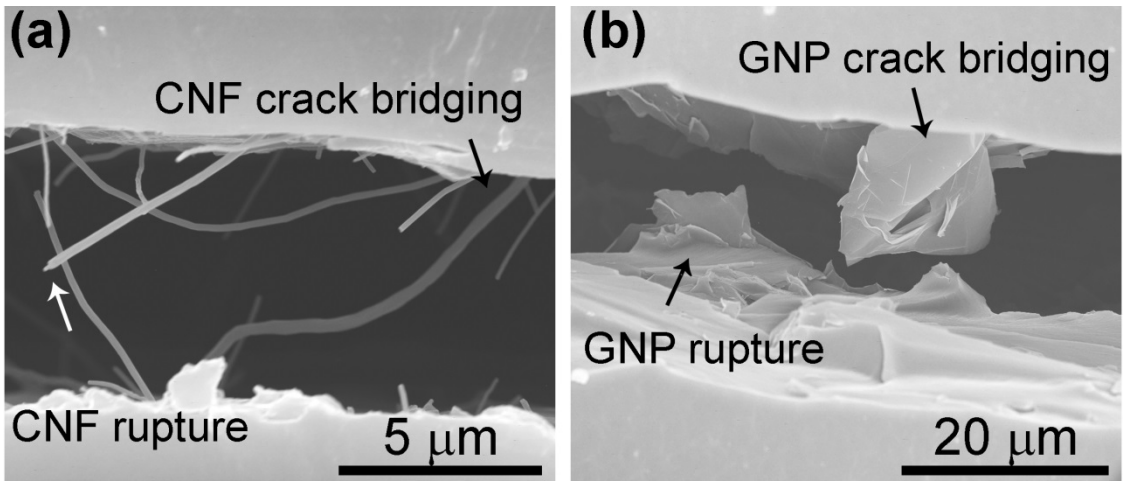

Fig. 6 SEM image of the crack bridging by the nanofiller in the epoxy nanocomposites containing: (a) 1.0 wt% CNFs and (b) 1.0 wt% GNPs.

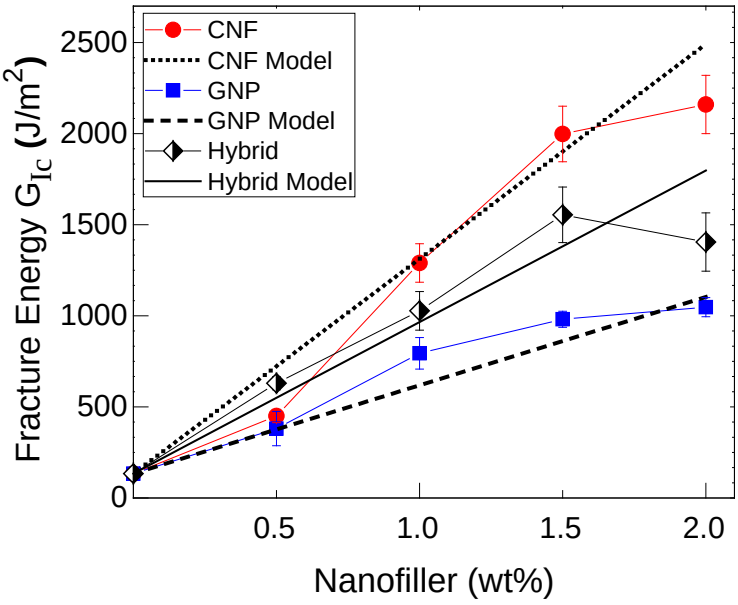

1

2 Fig. 7 Comparison of the experimental and theoretically-calculated fracture energies for the epoxy

3 nanocomposites. (Note: The hybrid nanocomposite wt% consists of a 1:1 ratio of both nanofillers)

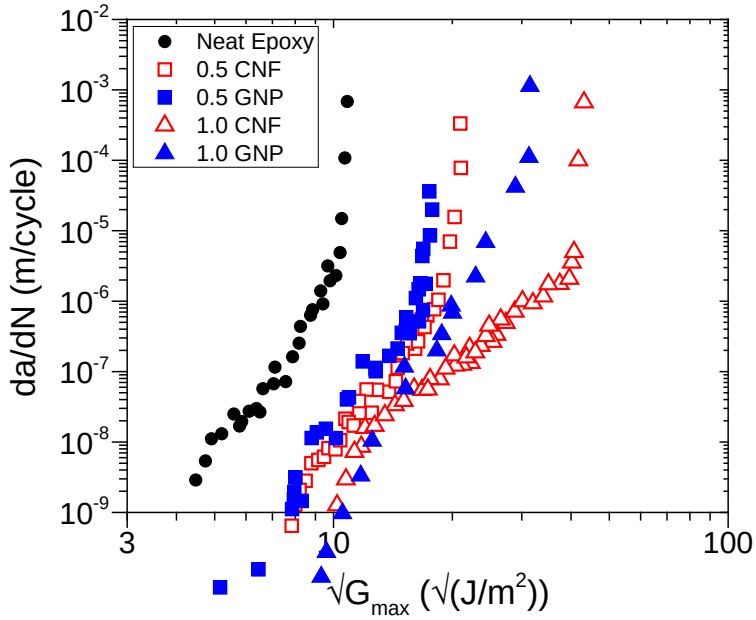

4

5 Fig. 8 Fatigue crack growth results showing the effects of the type and concentration of nanofiller on the

6 cyclic-fatigue resistance of the epoxy nanocomposites. The fatigue curve for the unmodified (i.e. neat)

7 epoxy is also shown.

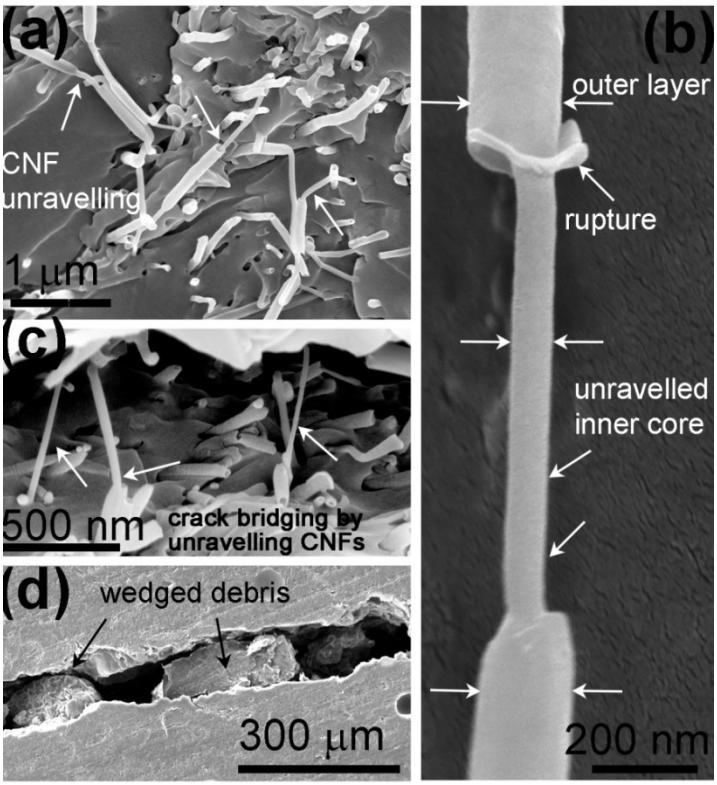

Fig. 9 (a-b) SEM image of the fracture surfaces of the CNF-epoxy nanocomposites showing the fatigue induced damage to the CNFs. (c) Side-view SEM image of the CNFs bridging a fatigue crack via an unravelling deformation mechanism of the inner helical core in the CNF-epoxy nanocomposites. (d) Side-view SEM image of debris particles in a fatigue crack which induce a shielding effect in the GNP-epoxy nanocomposites.

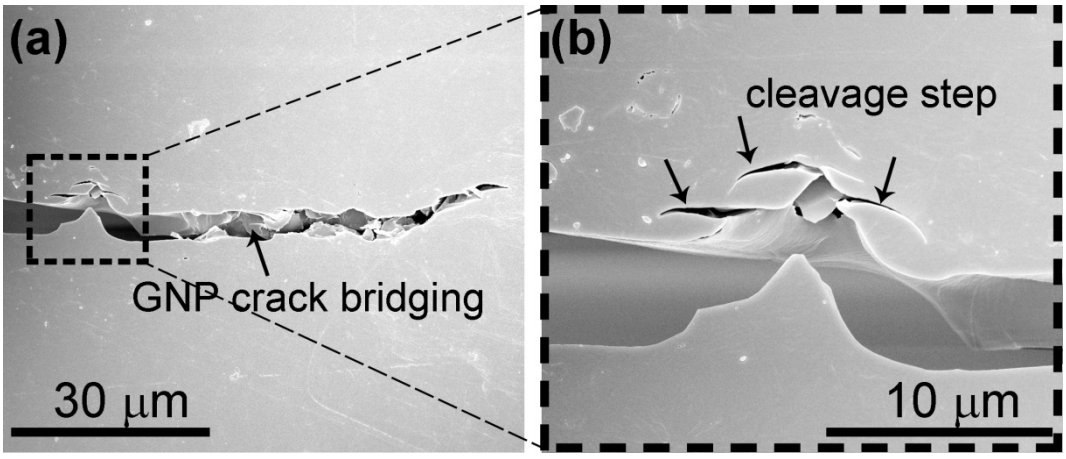

Fig. 10 (a-b) SEM image showing the side-view of the crack front of the epoxy nanocomposites containing 1 wt% GNPs.

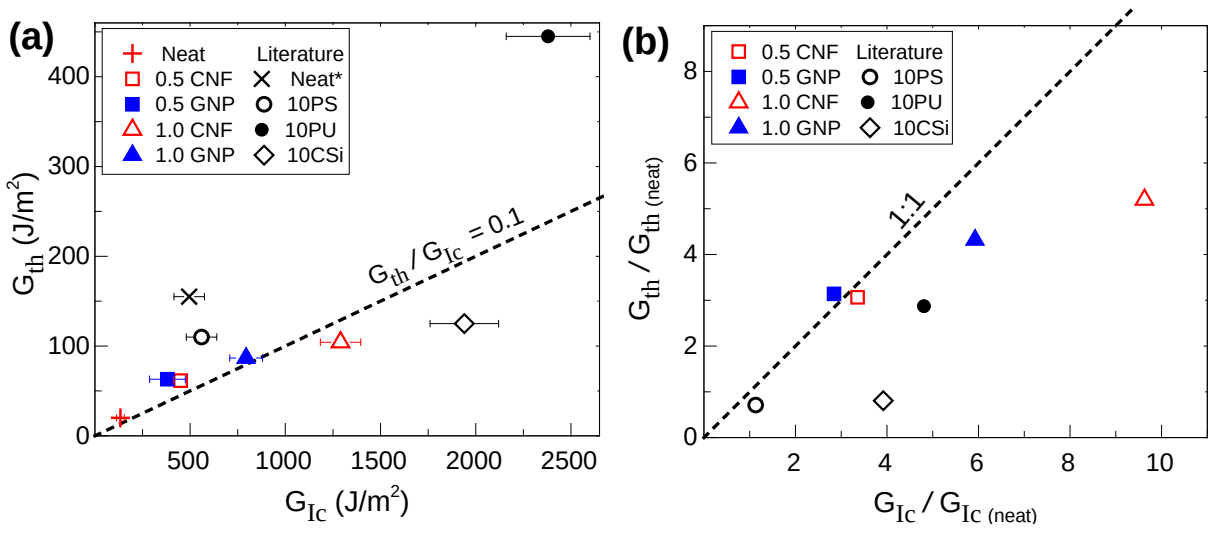

Fig. 11 (a) Threshold value, G_{th}, from the cyclic-fatigue tests versus the quasi-static fracture energy, G_{Ic}, for the present epoxy nanocomposites and a comparison to the data from Kinloch et. al. [56] for an diglycidyl ether of bis-phenol A (DGEBA) epoxy polymer modified with 10 wt% of a difunctional epoxydised polysulfide (10PS), 10 wt% of a poly(propylene glycol)-based polyurethane (10PU), and 10 wt% of core-shell rubber particles (consisting of a polybutadiene core with a functionalised poly(methyl methacrylate) shell) (10CSi). The results shown in (b) are normalised by the value of G_{th} or G_{Ic}, as appropriate, of the respective unmodified (i.e. neat) epoxy. (The dashed lines in Figs. 11 (a-b) are merely to aid interpretation of the results).

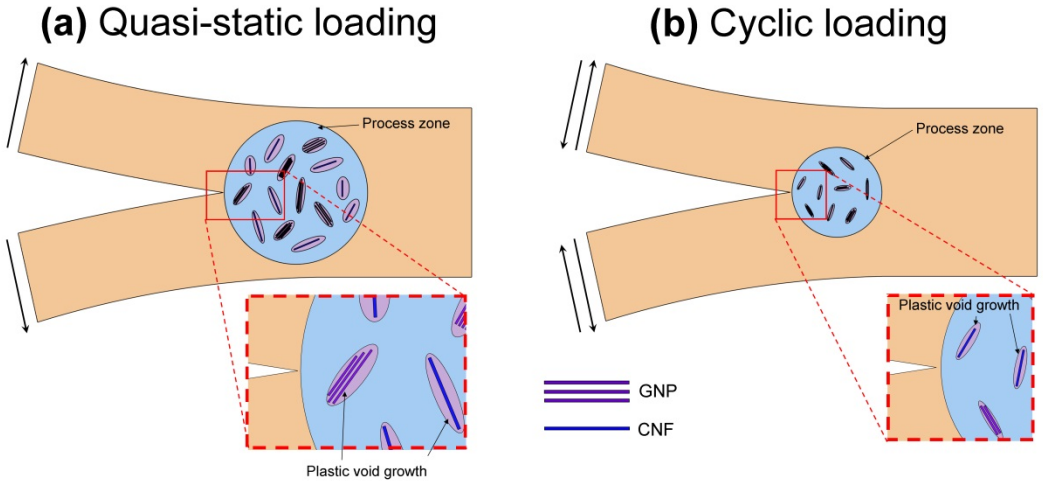

Fig. 12 Schematic representations of the effects of the loading conditions on the process zone size in the epoxy nanocomposites.

Table 1. Definition and list of values for the various parameters used in the fracture modelling.

Parameter	Symbol	Unit	Value	Source
CNF diameter	d_f	nm	135	[36]
CNF average length after dispersion	l_f	μm	20	[9]
GNP thickness	t	nm	10	[37]
GNP width	W	μm	25	[37]
GNP length	l	μm	25	[37]
CNF tensile strength	σ_f	GPa	8.7	[36]
GNP tensile strength	σ	GPa	5	[37]
Young's modulus of the CNF	E_f	GPa	320	[38]
Young's modulus of the GNP	E_G	GPa	1000	[38]
Density of the CNF	ρ_f	kg/m^3	1400	[36]
Density of the GNP	ρ	kg/m^3	2200	[37]
Density of the unmodified epoxy	ρ_m	kg/m^3	1011	[39]
CNF/epoxy interface strength	τ_i	MPa	25	[40]
GNP/epoxy interface strength	τ_G	MPa	2.3	[40]
Interfacial fracture energy of the nanofiller/epoxy interfaces	G_i	J/m^2	3.3	[9]
Tensile yield strength of unmodified epoxy	σ_y	MPa	50.5	[39]
Young's modulus of unmodified epoxy	E_m	GPa	3.17	[39]
Fracture energy of the unmodified epoxy	G_{CU}	J/m^2	134	-
Plastic zone size of unmodified epoxy	r_{yu}	μm	10	[9]
Pressure-dependent yield-stress constant	μ_m	-	0.2	[41]
Maximum von Mises stress concentration	K_{vm}	-	2.11	[27]

Table 2. Contributions to the fracture energy, G_{Ic}, of the epoxy nanocomposites from the various toughening mechanisms which were identified, as calculated using the fracture model.

Nanofiller	**Concentration** (wt%)	$\Delta G_{\text{pull-out}}$ (J/m^2)	$\Delta G_{\text{rupture}}$ (J/m^2)	ΔG_{db} (J/m^2)	ΔG_{v} (J/m^2)
CNFs	0.5	210	10	1.2	369
	1.0	420	19	2.4	737
	1.5	630	29	3.5	1106
	2.0	839	39	4.7	1474
GNPs	0.5	149	0.9	20	73
	1.0	298	1.7	39	146
	1.5	446	2.6	59	219
	2.0	595	3.4	79	292